



Synthesis of boron nitride nanotubes using triple DC thermal plasma reactor with hydrogen injection

Minseok Kim^a, Yong Hee Lee^a, Jeong-Hwan Oh^a, Seung-Hyun Hong^a, Byeong-Il Min^{a,1}, Tae-Hee Kim^{b,*}, Sooseok Choi^{a,b,*}

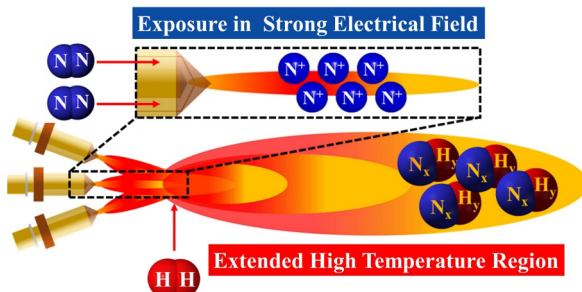
^a Department of Nuclear and Energy Engineering, Jeju National University, Jeju 63243, Republic of Korea

^b Major of Energy and Chemical Engineering, Faculty of Applied Energy System, Jeju National University, Jeju 63243, Republic of Korea

HIGHLIGHTS

- Boron nitride nanotubes were synthesized using direct current thermal plasma.
- Triple torch configuration was applied to synthesis reactor.
- Role of hydrogen was analyzed chemically and physically.
- A superior yield of 0.59 g/h-kW for boron nitride nanotubes was achieved.

GRAPHICAL ABSTRACT



ARTICLE INFO

Keywords:
Triple DC thermal plasma reactor
Boron nitride nanotubes
Synthesis
Hydrogen
Thermodynamic equilibrium equation
Numerical analysis

ABSTRACT

Highly crystalline boron nitride nanotubes (BNNTs) having multi-walls (≤ 5 walls) and a small diameter (~ 7 nm) were synthesized using a triple DC thermal plasma reactor with hydrogen injection. Triple torch configuration not only generates larger high temperature regions than single torch but also allow precursors to directly penetrate the core of the plasma flame, the hottest area in the reactor. A triple torch increases the productivity of BNNT synthesis by preventing the flow of precursors into the rim of plasma flame, a problem that occurs with single torch due to the high velocity and viscosity of the central flame. The role of hydrogen in the growth of BNNTs was analyzed by thermodynamic equilibrium reaction calculations and numerical analysis of thermal flow in the system. The reaction calculations revealed that hydrogen facilitates the formation of NH , NH_2 , and N_2H_2 molecules by inhibiting N from recombining into N_2 in the high temperature region. Hydrogen influences the formation of scattered high temperature and enthalpy regions due to its thermal properties and expands the vortex region, leading to longer residence times for B-N-H intermediates in the reactive region. As a result, 12.6 g of BNNTs are produced with 21.4 kW of input power. A comparison with other methods shows that this yield is superior and provides an economic perspective for the proposed pilot synthesis of BNNTs.

1. Introduction

The existence of boron nitride nanotubes (BNNTs) was first hypothesized in 1994 and proposed that BNNTs would be as structurally

stable as carbon nanotubes (CNTs) [1]. At that time, BNNTs evoked considerable interest because quasi-particle calculations suggested that single and multi-walled BNNTs are semiconducting with a high bandgap of 5.5 eV, that is independent of radius, helicity, and coaxial

* Corresponding authors at: Major of Energy and Chemical Engineering, Faculty of Applied Energy System, Jeju National University, Jeju 63243, Republic of Korea.
E-mail addresses: taeheekim@jejunu.ac.kr (T.-H. Kim), sooseok@jejunu.ac.kr (S. Choi).

¹ Current affiliation: Department of Chemical System Engineering, Kyushu University, Fukuoka, 819-0395, Japan.

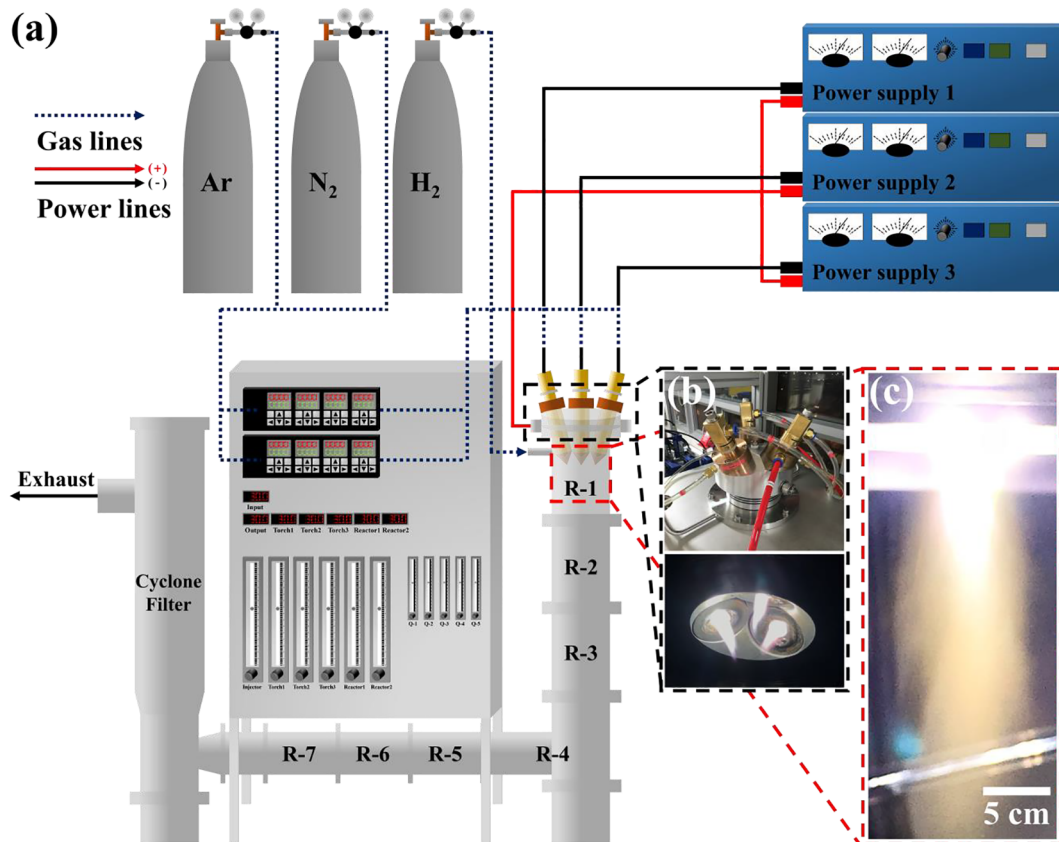


Fig. 1. Schematic diagram (a) of the triple DC thermal plasma reactor. Picture (b) of the upper part of triple thermal plasma system and operating triple thermal plasma torch. Picture (c) of a merged triple thermal plasma jet flame whose length reaches 30 cm.

arrangement, a property that is not seen in CNTs [2,3]. Synthesis of multi-walled BNNTs using carbon-free plasma discharge was first reported in 1995 [4], and many properties of the BNNTs were demonstrated: elastic mechanical properties [5–7], electron and field emission properties [8,9], electric piezoelectricity [10], thermal stability [11], optical properties [12–15], thermal conductivity [16,17], purification parameters [18–20], biocompatibility [21], and a partially ionic structure [22]. These properties make BNNTs attractive molecules for industrial use in optoelectronic devices, heat-resistant and piezoelectric materials, and as reinforcements for structural composites [23–26]. Despite the avid interest in BNNTs, a major impediment to using them in industrial applications is a low production rate; therefore, recent research has focused on the development of BNNT synthesis systems at a large scale.

Various methods that have been used to synthesize BNNTs can be categorized as high temperature synthesis and medium/low temperature synthesis using arc discharge [27–30], laser ablation/vaporization [31–35], chemical vapor deposition [36–39], ball milling with annealing [40–42], and template conversion [43,44]. From these works, it appears that synthesis of BNNTs is commonplace at laboratory-scale but remains difficult at pilot-scale, and the amount and quality of the produced BNNTs are inferior to those achieved with CNTs.

Regarding mass production of BNNTs, Smith *et al.* produced 60 mg of extraordinarily long and highly crystalline BNNTs without a catalyst in 30 min using laser ablation [45]. Huang *et al.* reported the production of ~50 mg of BNNTs with an average diameter of below 10 nm and lengths that ranged up to tens of μm in 3 h using chemical vapor deposition [39]. These techniques have improved the laboratory-scale production of BNNTs, but a noteworthy advance in BNNT production that can scale to industrial production level was recently achieved using induction thermal plasma process. This process continuously produced highly crystalline, small-diameter BNNTs at a rate approaching 20 g/h

with the help of hydrogen [46]. Previous works [41,42] introduced gases containing hydrogen to control the distribution of diameter during the synthesis of BNNTs, but no significant influence on mass production was reported. However, Kim *et al.* concluded that the addition of hydrogen as a reactant gas was an essential factor in achieving high-quality and high-yield growth of BNNTs [46,47].

In this work, we propose a system that is highly suitable for pilot-scale synthesis of BNNTs. A triple torch is introduced into DC thermal plasma reactor to produce a large coalesced area of high temperature that allows precursors to penetrate the merged plasma flame easily [48–51]. To grow into nanoparticles, precursors must remain within a high temperature area long enough to be evaporated. This is difficult in single torch thermal plasma because the high velocity and viscosity within a single plasma flame causes precursors to flow to the rim of the flame [52]. Additionally, a triple torch thermal plasma reactor produces small-diameter BNNTs because the DC plasma jet provides a higher rate of quenching than induction plasma. The effects of hydrogen in the BNNT synthesis system was investigated chemically and physically. The Gibbs free energy for the chemical reactions was calculated, and the thermal flow environment during BNNT synthesis reactor was numerically simulated. Furthermore, we compared production rate of BNNTs obtained with the proposed reactor with other methods relative to the input power and nitrogen consumption of the nitration reactant.

2. Experimental details

2.1. Thermodynamic equilibrium calculations

The proposed process of BNNT synthesis was investigated theoretically by conducting thermodynamic equilibrium calculations for each step of BNNT formation from precursor to B-N-H intermediates using HSC Chemistry software (Ver. 9.1.1, Outotec Research Oy, Finland).

The change in Gibbs free energy within a given temperature range indicates whether the reaction is a spontaneous chemical reaction [53]. To theoretically explain why injection of H₂ gas is essential to the proposed BNNT synthesis, the thermodynamics of reactions that form NH and BH gases were calculated with H₂ gas. Subsequently, the thermodynamics of reactions that form boron nitride hydrogen (BNH and BNH₂) were calculated with the formed NH and BH gases. In these chemical reactions, the temperature range was 500 K–10,000 K, and pressure was fixed at atmospheric pressure.

2.2. Synthetic experiment of boron nitride nanotubes

A schematic diagram of the triple DC thermal plasma reactor used to synthesize the BNNTs is shown in Fig. 1(a). The system consists of three thermal plasma torches (Plasniax Co., Ltd., Republic of Korea), vertical reactors (R-1, R-2, and R-3) and horizontal reactors (R-4, R-5, R-6, and R-7), three DC power supplies, a cyclone filter, and a control box of cooling waters and gases. A picture of the triple torch configuration (top image) and the triple thermal plasma jet (bottom image) when each plasma flame is formed with Ar gas is shown in Fig. 1(b). A merged triple thermal plasma jet formed with Ar-N₂ mixed plasma forming gas is shown in Fig. 1(c), demonstrating that the length of the plasma flame reaches 30 cm without the confinement chamber.

The experimental conditions are summarized in Table 1. The preliminary experiments for the torch operation were conducted according to the input power and gas usage. A single set of conditions is shown because the plasma flame was stable even after extended operation. Hexagonal boron nitride (h-BN) powder (~1 μm, 98%, 255475, Sigma-Aldrich, Inc., USA) was used as a precursor. Individual thermal plasma jets were generated by 4 L/min Ar and 8 L/min N₂ mixed gases under atmospheric pressure, and 8 L/min of H₂ as the reactant gas was injected from the upper part of R-1 (Fig. 1(a)). The input power of each torch was 6.9–7.5 kW at a fixed current of 100 A. The precursor was injected with 5 L/min of Ar gas into the coalesced plasma flame from the top of the triple torch, and the feeding rate was 0.5–0.6 g/min.

The crystal structure of the synthesized BNNTs was analyzed by X-ray diffraction (XRD) (Malvern Panalytical, Ltd, Empyrean, UK) with CuK_α radiation ($\lambda = 1.5406 \text{ \AA}$). The morphological properties and chemical composition of the synthesized BNNTs were analyzed using field emission scanning electron microscopy (FE-SEM) (MIRA3, TESAN, Czech) with energy dispersive spectroscopy (EDS) (X-max, Oxford Instruments, UK) at 15 kV accelerating voltage. The produced powder was coated by platinum using a sputter coater (Q150R S, Quorum, UK) to prevent electron charging at a fixed current of 20 mA for 30 s. Detailed stratified appearance such as multi-walled structures of the synthesized BNNTs were observed using field emission transmission electron microscopy (FE-TEM) (JEM-2100F, JEOL Ltd., Japan) at 200 kV accelerating voltage.

2.3. Numerical simulations

Numerical simulations were carried out to analyze the thermodynamic change inside the reactor from the injection of hydrogen

Table 1
Experimental conditions for the numerical simulation and synthesis of BNNTs.

| Experiment | Numerical simulation |
|---|---|
| Chamber pressure [kPa] | 101.325 |
| Plasma forming gas [slpm ^a] | 4 (Ar), 8 (N ₂) |
| Carrier gas [slpm] | 5 (Ar) |
| Reactant gas [slpm] | 8 (H ₂) |
| Arc current [A] | 100 |
| Arc voltage [V] ^b | (1) 70 (2) 69 (3) 75 (1) 67.2 (2) 67.2 (3) 67.2 |

^a slpm, standard liters per minute.

^b numbers refer to each torch (see Fig. 1b).

molecules. The boundary conditions of temperature and velocity for the thermal plasma jet emitted from the triple plasma torch were applied as inlet conditions to simulate the thermal flow inside the reactor. The arc discharge inside the torch was analyzed using a two-dimensional numerical code, DC Plasma Torch in Unstructured Grid System (DCPTUN) with magnetohydrodynamic (MHD) equations [54] because the electrical effect with the arc generated between the cathode and the anode had to be reflected in the case of the simulation for thermal plasma. The

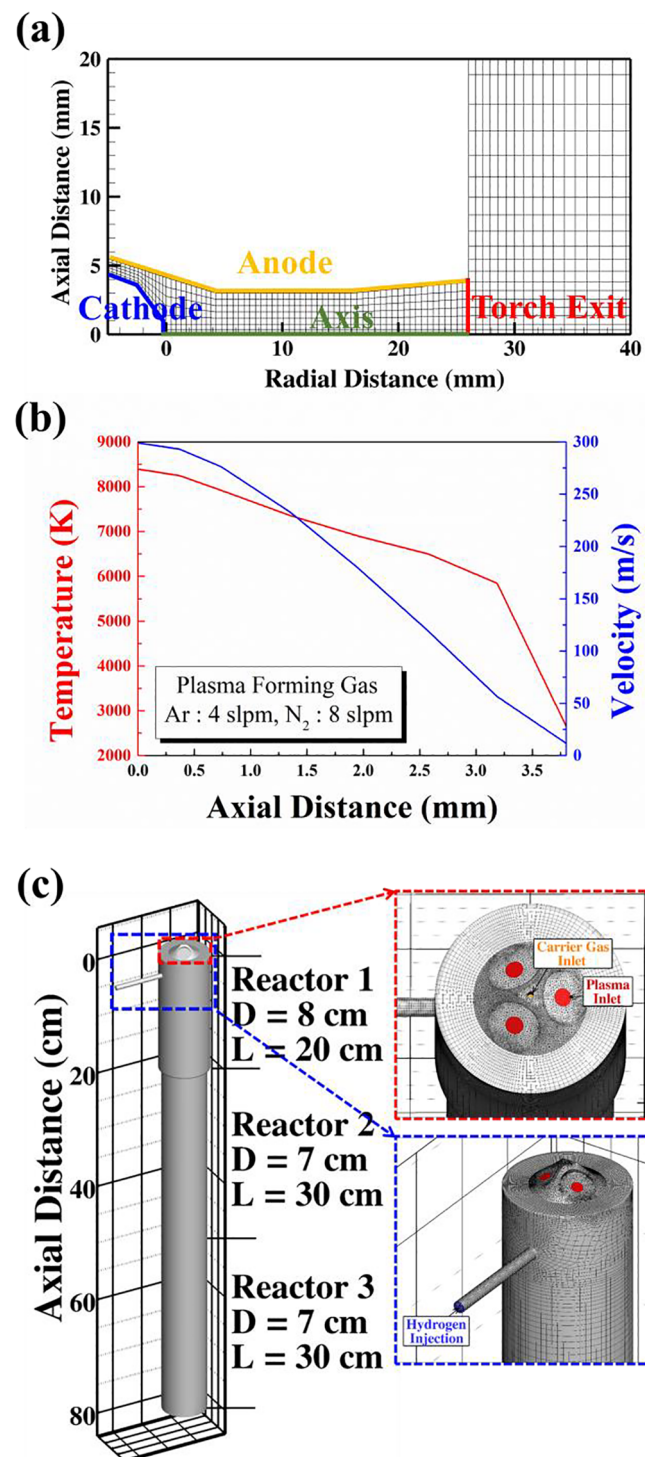


Fig. 2. Two-dimensional meshes (a) of the torch and the calculated temperature and velocity profile (b) of the torch exit in the torch region. Three-dimensional mesh (c) of the simulated reactor (R-1, R-2, and R-3), triple torch, precursor, and hydrogen gas inlet nozzle configuration used to simulate the reactor region.

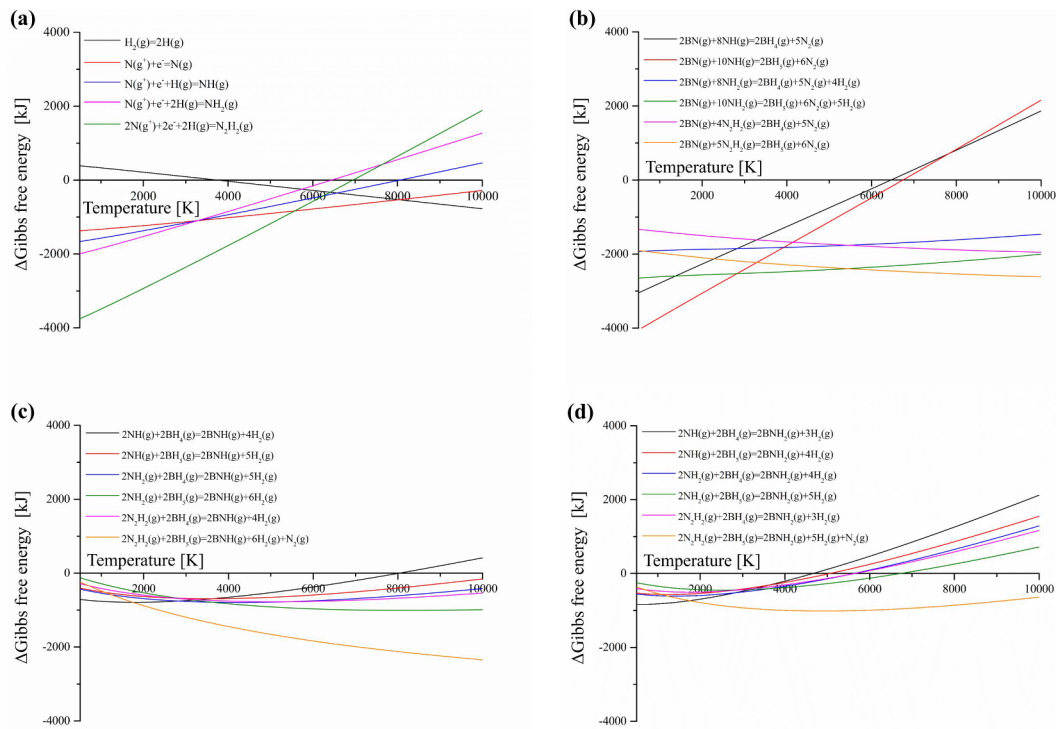


Fig. 3. Thermodynamic equilibrium calculations for the BNNTs synthesis process. (a) NH, NH₂, and N₂H₂ gas formations from decomposed N radical ions. (b) BH₄ and BH₅ gases formation reactions from BN gas and the formed NH, NH₂, and N₂H₂ gases. (c) BNH and (d) BNH₂ formation from the formed BH₄ and BH₅ gases and the formed NH, NH₂, and N₂H₂ gases.

interaction between the plasma forming gas and the arc was described using the DCPTUN based on several assumptions: optically thin, electrically neutral, turbulent, and under local thermodynamic equilibrium (LTE). The high temperature thermodynamic and transport properties of the processing gas under LTE was obtained from a previously reported thermodynamic database [55].

Mass, energy, and momentum conservation equations were solved for torch and reactor regions by employing the *k*-*e* turbulence model to consider the turbulence generated by a plasma jet having a steep temperature gradient and rapid velocity [56]. A two-dimensional mesh was adopted because a single-torch has the axis-symmetric geometry shown in Fig. 2(a). The torch exit temperature and velocity profiles calculated using the DCPTUN are shown in Fig. 2(b), and are applied as inlet conditions for the reactor region. A high temperature distribution above 2000 K with a maximum temperature of 8392 K is formed at the torch exit, and the velocity of the plasma jet reaches 299 m/s. The numerical simulation was conducted with conditions equal to the experiment in Table 1. A single torch was simulated and the calculated temperature and velocity profile were applied identically to the three torches. The calculated voltage is 67.2 V, which has an error of

approximately 5% relative to the measured average voltage of 71.3 V.

The calculated temperature and velocity profiles (Fig. 2b) at the torch exit were applied as inlet boundary conditions for the numerical simulation of the reactor by a commercial computational fluid dynamics code, ANSYS-FLUNET (Ver. 19.2) [57,58]. The electrical effect was considered in the torch regions, but the reactor region was regarded as a thermal fluid based on the torch exit conditions, such as temperature and velocity of the plasma jet, without considering electrical effects because the primary cause of the chemical reaction in thermal plasma is high thermal energy. Therefore, the thermal environment inside the reactor was analyzed to understand thermodynamic changes with and without the injection of hydrogen molecules. The general mass, momentum and energy equations were included in the reactor simulation, and the *k*-*e* turbulence model employed were the same as those used in the simulation of the torch region.

The reactor geometry was constructed as a three-dimensional mesh due to the triangle arrangement of the triple torch. The three-dimensional mesh containing the triple torch, a carrier gas nozzle, and a hydrogen gas inlet nozzle is shown in Fig. 2(c). The diameter of the

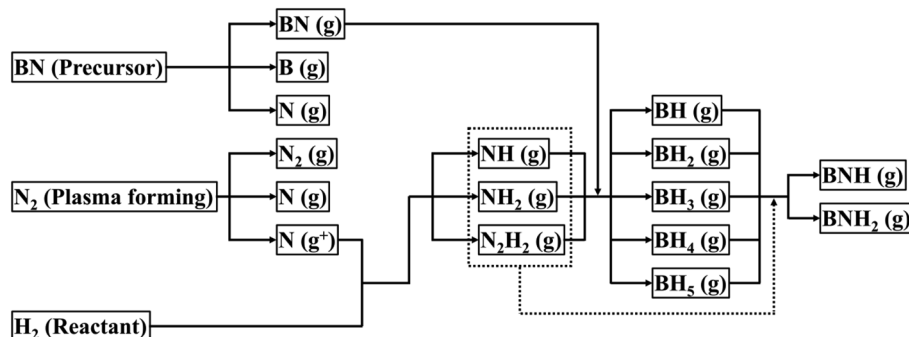


Fig. 4. Proposed chemical reaction pathways for the synthesis BNNTs with precursor of h-BN, plasma forming gas of N₂, and reactant gas of H₂.

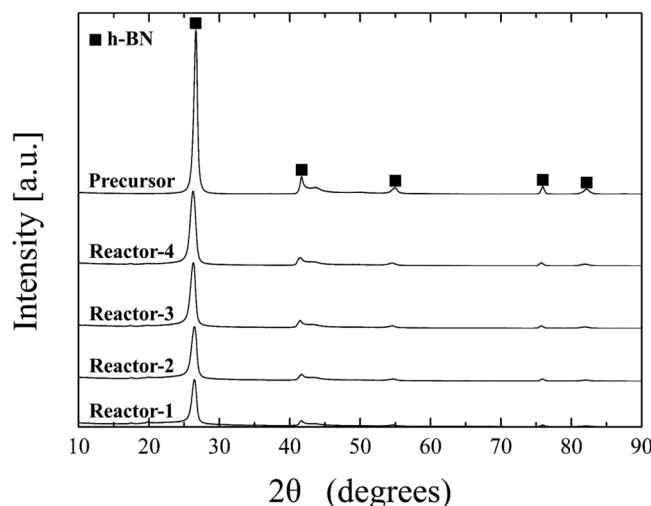
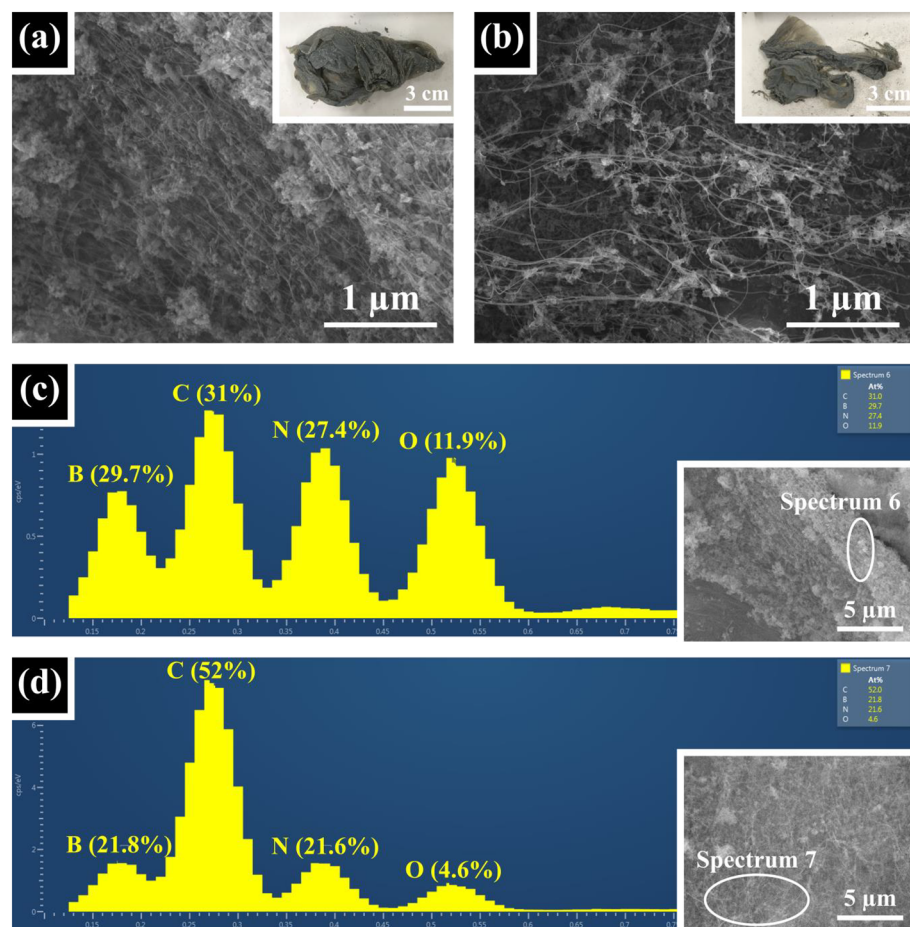


Fig. 5. X-ray diffraction (XRD) patterns of h-BN precursor and synthesized BNNTs at the vertical reactor from R-1 to R-4.

carrier gas nozzle and the torch nozzle are 2.5 mm and 7.6 mm, respectively. Each torch has a slope of 25° relative to R-1. The hydrogen gas inlet nozzle has a diameter of 7.8 mm and is located 2.6 cm below the top of R-1. The most complicated thermal flow is generated in R-1–3 because the inflow of plasma forming and H₂ gas were encountered in R-1 nearby the plasma flame, and knowing the spatial flow and temperature distribution is vital to understanding the process of BNNT synthesis. Therefore, only R-1, R-2, and R-3 were numerically simulated to observe the thermal flow inside the reactor.



3. Results and discussion

3.1. Thermodynamic equilibrium calculation

Nitrogen is an essential source for BNNT growth; it decomposes and quickly recombines into N₂ in the high temperature (< 7000 K) region. The direct nitration of B with N₂ dissociation to form an h-BN phase rarely occurs and is extremely slow due to the strong triple bond of nitrogen molecules. However, hydrogen prevents nitrogen atoms from recombining to N₂; instead, NH, NH₂, and N₂H₂ gases are formed in the high temperature region provided by a merged plasma flame.

The reactions that occur with ionized nitrogen with hydrogen under 10,000 K are shown in Fig. 3(a). Nitrogen molecules form N⁺ ions through direct ionization of N, (N + N + e → N⁺ + 2e, with a threshold energy of 14.5 eV) and dissociative ionization of N₂ molecules, (N₂ + e → N⁺ + N + 2e, with a threshold energy of 24.3 eV) are ionized in an electrical field that is strong enough to ionize them when they are injected as plasma forming gas and generates an arc [59–61]. These ionizations are highly dominant in the high electrical field between the cathode and anode of each torch so that it is regarded that N⁺ ions participated in reaction to form N_xH_y molecules [62]. The red line in Fig. 3(a) indicates the recombination between N radical ions and electrons. The blue, magenta, and green lines represent N_xH_y molecule formation from the reaction between B radical ions and hydrogen. At temperature below 5072 K, the junction point of the red and green lines, the Gibbs free energy of the green line is lower than that of the red line, meaning that N₂H₂ formation is dominant from 3743 K, the temperature at which hydrogen atoms recombine, to 5072 K. The gas phase is represented as (g) and radical ions are represented as (g⁺). These results show that the presence of hydrogen plays an essential role in the production of NH, NH₂, and N₂H₂ gases. The formed NH₂ and N₂H₂ molecules actively combine with BN gas, yielding BH₄ (blue and magenta

Fig. 6. Scanning electron microscopy (SEM) and macroscopic images and energy dispersive spectroscopy (EDS) analysis of the grown boron nitride nanotubes (BNNTs) according to the reactor. SEM and macroscopic; images of BNNTs collected at the (a) vertical reactor and (b) horizontal reactor; EDS results for synthesized BNNTs collected at the (c) vertical reactor and (d) horizontal reactor.

lines) and BH_5 (green and orange lines) gases that are produced throughout the temperature range. This suggests that BN gas also plays an important role in the formation of BH_4 and BH_5 gases. BNH gas is formed by reactions between the formed BH_4 and BH_5 gases and the formed N_xH_y molecules, as shown in Fig. 3(c). In particular, BH_4 (blue and magenta lines) gas primarily combines with NH_2 and N_2H_2 gases, and BH_5 (green and orange lines) gas reacts preferentially with NH_2 and N_2H_2 gases to generate BNH under 10,000 K. BNH_2 gas formation reactions from the formed BH_4 and BH_5 gases and the formed NH , NH_2 , and N_2H_2 gases are shown in Fig. 3(d). BH_5 (orange line) shows the lowest Gibbs free energy in the Fig. 3(d). These results suggest the reaction of N_2H_2 with BH_5 gas is crucial to the generation of the BNNTs because BNH and BNH_2 gas eventually produce BNNTs through a dehydrogenation reaction and formation of a boron droplet by nucleation [47]. Moreover, B-N-H intermediates are slightly more dominant than BNH_2 gas molecules. The chemical reaction pathway of BNNT synthesis from the plasma forming gas of N_2 , the precursor of BN, and the reactant gas of H_2 to BNH and BNH_2 is summarized in Fig. 4. These findings indicate that the reactions that form NH , NH_2 , and N_2H_2 proceed primarily by the hydrogen-rich atmosphere; these reaction products are crucial for the formation of diverse BH gases and B-N-H intermediates (i.e., BNH and BNH_2) that ultimately grow into BNNTs.

3.2. Synthesis of boron nitride nanotubes

XRD analysis of collected samples identify them as h-BN structures by the similarity of XRD pattern to those of the precursor, as shown in Fig. 5. The crystallinity of the synthesized BNNTs improve slightly as they move through the plasma flame, showing the correlation between residence time and the crystallinity of the resulting BNNTs. SEM images with macroscopic images of the BNNTs collected from the vertical and horizontal reactors are shown Fig. 6(a) and (b), respectively. A fabric material appearing as tangled threads successfully formed in the triple DC thermal plasma reactor, showing a thin cotton appearance at the macroscopic scale. In addition, the length of the fabric material emerging from the horizontal reactors (Fig. 6(b)) is much longer than that emerging from the vertical reactors (Fig. 6(a)), which suggests that the residence time of the precursor in the reactor influences the length of the grown BNNTs. The vertical reactors are closer to the plasma flame, meaning that the grown BNNTs in these reactors have less time to grow than the BNNTs in the horizontal reactors, as seen from the XRD patterns. This suggests that residence time influences crystallinity of the synthesized BNNTs as well as length. EDS analysis provides the chemical composition of the BNNTs from the vertical and horizontal reactors, as shown in Fig. 6(c) and (d), respectively. The results show that the BNNTs from both reactors have almost identical ratios of boron and nitrogen. This suggests that boron and nitrogen are the component species of the fabric material, although a carbon peak was also observed, which likely came from the carbon tapes used for in the SEM analysis.

TEM analysis validated that the fabric material from the vertical and horizontal reactors has tubular structures that are straight and parallel to the axis of the tube, as shown in Fig. 7. Some single-walled BNNTs are observed, but the number of walls most frequently observed is 2 and 3, and majority of the BNNTs are three-walled. The D_{50} of tubular structures is 7.05 nm (4.7 nm of Pt thickness by the sputter coater is considered). In addition, the multi-walled BNNTs have a highly crystalline structure with no evidence of the bamboo structures that result from relatively low temperature synthesis [41,42]. These highly crystalline structures emerge from a thermal plasma synthesis process that provides enough time for B-N-H intermediates to form crystal structures in the high temperature region [28–30]. Previous studies discussed the role of hydrogen on diameter distribution in the grown BNNTs, but did not mention a role in the scale of synthesis [41,42]. By adding hydrogen gas to the synthesis of the BNNTs, the reaction presented in this study generates a high-yield rate of 12.6 g/h without metal catalysts. Previous work has achieved a prominent achievement of higher yield rate approaching 20 g/h [46]. However, it is important to consider the cost-effectiveness of a synthesis system, such as how much power and gas are

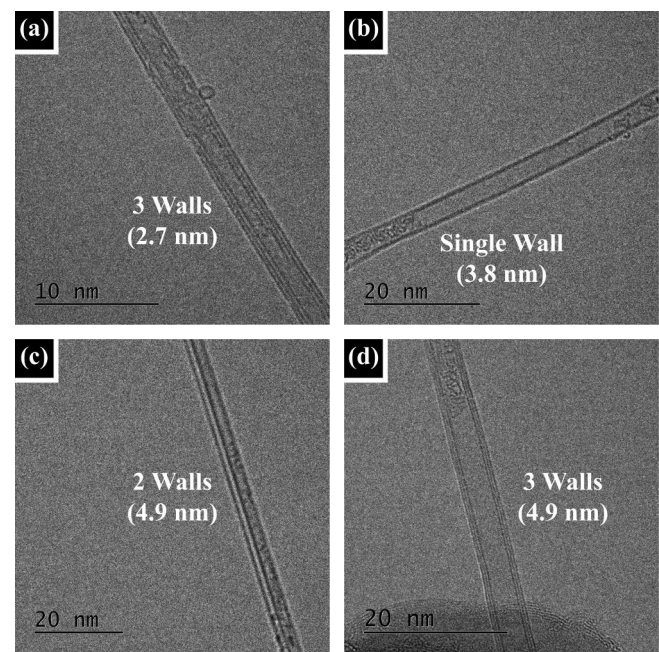


Fig. 7. HR-TEM images of the synthesized BNNTs according to the reactor. (a) A three-walled BNNT whose diameter is approximately 2.7 nm, and (b) a single-walled BNNT whose diameter is approximately 3.8 nm from the vertical reactor. (c) A double-walled BNNT whose diameter is approximately 4.9 nm, and (d) a triple-walled BNNT whose diameter is approximately 4.9 nm from the horizontal reactor.

employed in the synthesis system, to move toward practical application. A comparison of production rate per input power and usage of nitrogen gas for the various BNNT synthesis methods is summarized in Table 2. The comparison shows 1 kW of input power per hour was consumed to synthesize 0.59 g of BNNTs in this work, which is 1.8 times that of induction thermal plasma synthesis.

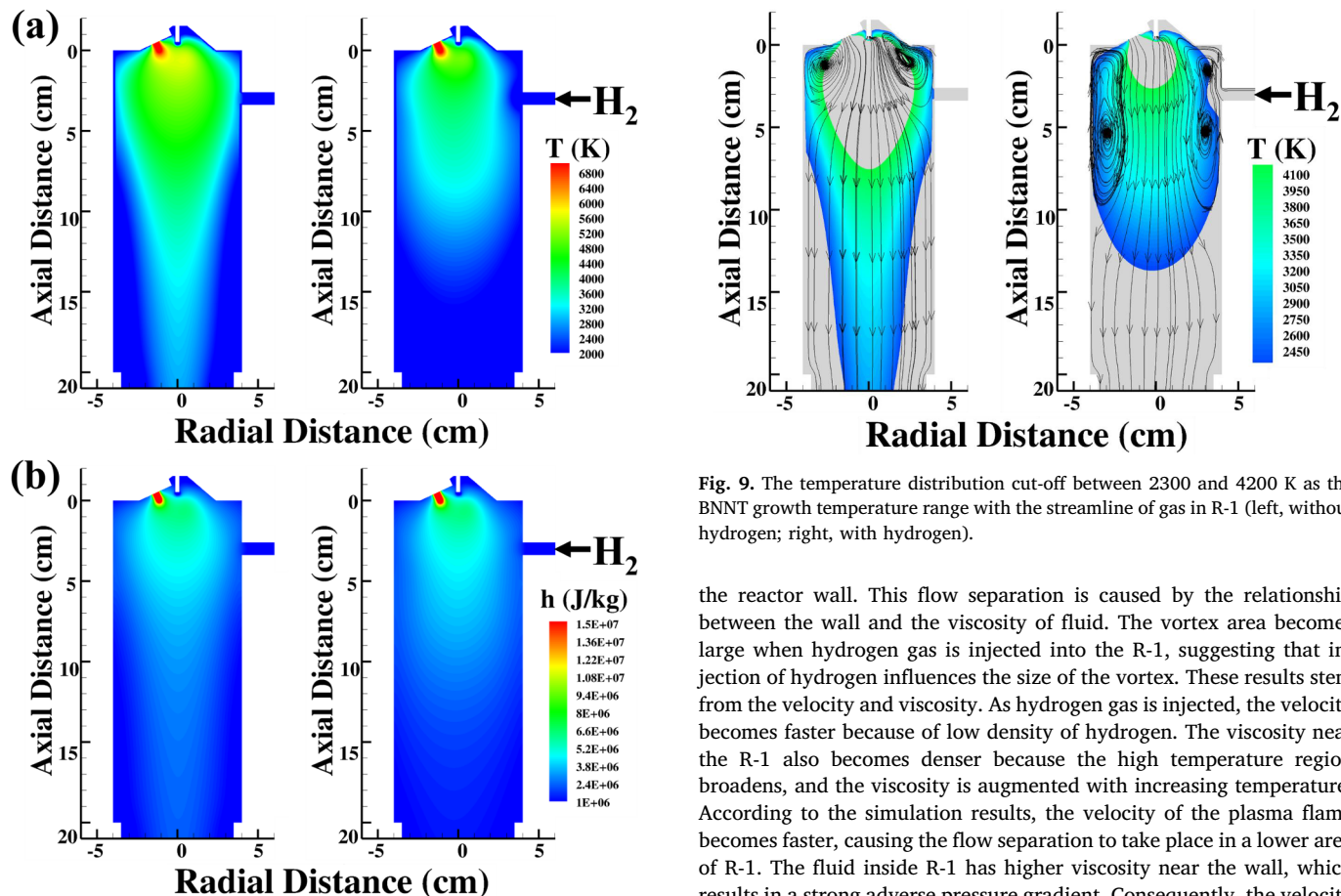
3.3. Numerical analysis of thermal plasma flow

Hydrogen gas not only plays an essential chemical role in the BNNT growth process, but it also influences the physical flow of the plasma flame in the reactor. Firstly, the change due to injection of hydrogen gas was examined from the perspective of energy in the Fig. 8, which shows the temperature and enthalpy distributions with and without the injection of hydrogen. Although the total power supplied inside the reactor is equal, a difference in temperature distribution occurs due to the injection of hydrogen as the reactant gas. As shown in the Fig. 8(a), the high temperature area (> 3000 K) was shorter and the plasma tail was broader when hydrogen gas is injected, which means that the heat in the area faster transfer to the surroundings such as inner wall of reactor. This phenomenon stems from the fact that the thermal conductivity of hydrogen gas is higher than nitrogen gas throughout the temperature range [55,63]. The change in enthalpy distribution due to hydrogen injection exhibits a trend similar to the temperature distribution, having a broader tail and a shorter flame as shown in Fig. 8(b). Despite having a higher enthalpy value at the same temperature, the hydrogen gas does not contribute to an increase in total enthalpy inside the reactor; rather it plays a quenching role. This means that hydrogen gas has no impact on the consumed power because a relatively low amount of the hydrogen gas is employed as the reactant gas. Therefore, the injection of hydrogen as the reactant gas shortens and broadens the energy distribution, suggesting that hydrogen cool the reactor. This causes a reduction in the area of the high temperature region, which seems to be unfavorable for BNNT formation because BNNTs are able to grow well at the relatively high temperature [47]. Nevertheless, BNNTs are produced successfully, which is explained by the aspect of flow.

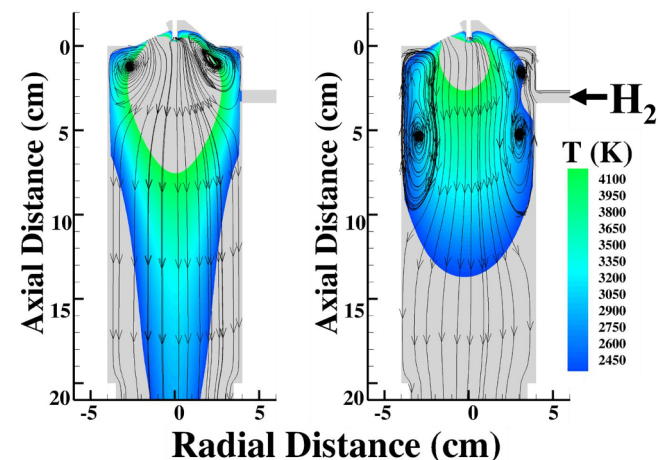
Table 2

Comparison of production rate per input power and usage of nitrogen gas for various BNNT synthesis methods.

| Method | Input power (kW) | Production rate (g/h) | Production rate per power (g/h·kW) | Injection gas (slpm ^a) | Production rate per nitrogen gas (g/h·slpm) | Reference |
|--------------------------------|------------------|-----------------------|------------------------------------|--|---|--|
| Laser ablation | 1–1.2 | 0.5–0.55 | 0.417–0.55 | N ₂ : 4.8–7.2 | 0.07–0.11 | Arenal, R. et al [35] Smith, M. W. et al [45] |
| | 1 | 0.12 | 0.12 | – | – | |
| Chemical vapor deposition | – | 0.2 | – | – | – | Kim, M. J. et al [38] Huang, Y. et al [39] |
| | – | 0.016 | – | Ar: 0.3, NH ₃ : 0.2 | 0.08 | |
| RF ^b thermal plasma | 60 | 20 | 0.33 | Ar: 75, N ₂ : 55, H ₂ : 20 | 0.36 | Kim, K. S. et al [47] |
| | – | – | – | Ar: 12, N ₂ : 24, H ₂ : 8, | 0.525 | |
| DC ^c thermal plasma | 21.4 | 12.6 | 0.59 | – | – | Present work |

^a slpm, standard liters per minute.^b RF, radio frequency.^c DC, direct current.**Fig. 8.** (a) The temperature distribution and (b) the enthalpy distribution of R-1 with and without hydrogen gas (left figures, without hydrogen; right figures, with hydrogen).

Boron droplets are initiators of BNNT growth, being able to exist from nucleation temperature (4200 K) to solidification temperature (2300 K) [47]. In this work, BNNTs were massively produced under relatively low power although the temperature ranges from 2300 to 4200 K were not primarily formed as compared with previous works [46,47]. This phenomenon occurs because a vortex area inside R-1 contributes to the growth of the BNNTs despite the relatively low power. The streamlines with arrows as well as the temperature distribution between nucleation and solidification of boron are shown in Fig. 9. Regardless of whether hydrogen gas is present, vortex flow is created by the flow separation due to an adverse pressure gradient near

**Fig. 9.** The temperature distribution cut-off between 2300 and 4200 K as the BNNT growth temperature range with the streamline of gas in R-1 (left, without hydrogen; right, with hydrogen).

the reactor wall. This flow separation is caused by the relationship between the wall and the viscosity of fluid. The vortex area becomes large when hydrogen gas is injected into the R-1, suggesting that injection of hydrogen influences the size of the vortex. These results stem from the velocity and viscosity. As hydrogen gas is injected, the velocity becomes faster because of low density of hydrogen. The viscosity near the R-1 also becomes denser because the high temperature region broadens, and the viscosity is augmented with increasing temperature. According to the simulation results, the velocity of the plasma flame becomes faster, causing the flow separation to take place in a lower area of R-1. The fluid inside R-1 has higher viscosity near the wall, which results in a strong adverse pressure gradient. Consequently, the velocity magnitude of reverse flow near the wall is three times higher with the injection of hydrogen gas than without it. A large and strong vortex is created by injecting hydrogen gas makes the materials stay inside R-1, providing enough time for the materials to chemically interact. The majority of the vortex area is also generated in the region where the boron exits as droplets. Therefore, the vortex causes the B-N-H intermediates to reside in the reactive temperature region for an enough time to grow into the BNNTs. Subsequently, the BNNTs that grow in the vortex region naturally escape along the plasma flame owing to the inertial force of the BNNTs that are weighted by the continuous synthetic reaction.

4. Conclusions

Thermodynamic equilibrium reaction calculations, numerical simulations of thermal plasma flow, and synthesis experiments were

conducted to investigate the role of hydrogen in the efficient synthesis of multi-walled (≤ 5 walls) and small-diameter (~ 7 nm) BNNTs. The reaction calculations demonstrated that the injection of hydrogen as the reactant gas prevents the decomposed N from quickly recombining into N_2 and favors the formation of NH , NH_2 , and N_2H_2 gases. These gases generate various BH gases, which lead to the formation of B-N-H intermediates that eventually grow into BNNTs through dehydrogenation reactions with early nucleation of boron in the quenching process. The triple DC thermal plasma reactor that is divided into 7 regions provides an extensively coalesced high temperature area as well as a configuration that facilitates easy penetration of the precursor into the plasma flame. From these divided areas, it was determined that the residence time of the precursor influences the crystallinity and length of the grown BNNTs; length and crystallinity of the BNNTs increases as they move away from the plasma flame due to the low quenching rate. The correlation between BNNT formation and the numerical simulations inside the reactor supports the essential role of hydrogen. Because of the injection of the hydrogen gas, the reactive region has high temperatures and enthalpy dispersed over R-1. Hydrogen gas retains enthalpy and quickly transfers heat owing to the high thermal conductivity of hydrogen. The injection of hydrogen gas also causes a large vortex in the boron nucleation temperature region by causing the gases to swirl inside the R-1, which leads to longer residence times for gases and the precursor in the reactive region.

In conclusion, highly crystalline, small diameter (~ 7 nm), multi-walled BNNTs were synthesized in a triple DC thermal plasma reactor with low input power and gas usage. This efficient synthesis process contributes to the cutting-edge material industry because applications such as piezoelectric devices, the reinforcement of composite materials, and incorporation into aerospace materials to shield against neutrons are expected to exploit the compelling characteristics of BNNTs.

Declaration of Competing Interest

The authors declare that they have no known competing financial interests or personal relationships that could have appeared to influence the work reported in this paper.

Acknowledgments

This work was supported by the National Research Foundation, Republic of Korea (NRF-2018M3A7B4070992). Minseok Kim was supported by the Graduate Fellowship funded by the Hyundai Motor Chung Mong-Koo Foundation, Republic of Korea.

References

- [1] A. Rubio, J.L. Corkill, M.L. Cohen, Theory of graphitic boron nitride nanotubes, *Phys. Rev. B* 49 (1993) 5081–5084.
- [2] X. Blase, A. Rubio, S.G. Louie, M.L. Cohen, Stability and band gap constancy of boron nitride nanotubes, *Europhys. Lett.* 28 (1994) 335–340.
- [3] X. Blase, A. Rubio, S.G. Louie, M.L. Cohen, Quasiparticle band structure of bulk hexagonal boron nitride and related systems, *Phys. Rev. B* 7 (1995) 130–132.
- [4] N.G. Chopra, R.J. Luyken, K. Cherrey, V.H. Crespi, M.L. Cohen, S.G. Louie, A. Zettl, Boron Nitride Nanotubes, *Science* 269 (1995) 966–967.
- [5] N.G. Chopra, A. Zettl, Measurement of the elastic modulus of a multi wall boron nitride nanotube, *Solid State Commun.* 105 (1998) 297–300.
- [6] H.F. Bettinger, T. Dumitrićă, G.E. Scuseria, B.I. Yakobson, Mechanically induced defects and strength of BN nanotubes, *Phys. Rev. B* 65 (2002) 1–4.
- [7] D. Golberg, X.D. Bai, M. Mitome, C.C. Tang, C.Y. Zhi, Y. Bando, Structural peculiarities of in situ deformation of a multi-walled BN nanotube inside a high-resolution analytical transmission electron microscope, *Acta Mater.* 55 (2007) 1293–1298.
- [8] V. Meunier, C. Roland, J. Bernholc, M.B. Nardelli, Electronic and field emission properties of boron nitride/carbon nanotube superlattices, *Appl. Phys. Lett.* 81 (2002) 46–48.
- [9] J. Cumings, A. Zettl, Field emission and current-voltage properties of boron nitride nanotubes, *Solid State Commun.* 129 (2004) 661–664.
- [10] E.J. Mele, P. Král, Electric polarization of heteropolar nanotubes as a geometric phase, *Phys. Rev. Lett.* 88 (2002) 568031–568034.
- [11] Y. Chen, J. Zou, S.J. Campbell, G.L. Caer, Boron nitride nanotubes: pronounced resistance to oxidation, *Appl. Phys. Lett.* 84 (2004) 2430–2432.
- [12] J.S. Lauret, R. Arenal, F. Ducastelle, A. Loiseau, M. Cau, B. Attal-Tretout, E. Rosenthaler, L. Goux-Capes, Optical transitions in single-wall boron nitride nanotubes, *Phys. Rev. Lett.* 94 (2005) 1–4.
- [13] R. Arenal, O. Stéphan, M. Kociak, D. Taverna, A. Loiseau, C. Colliex, Electron energy loss spectroscopy measurement of the optical gaps on individual boron nitride single-walled and multiwalled nanotubes, *Phys. Rev. Lett.* 95 (2005) 1–4.
- [14] K. Watanabe, T. Taniguchi, H. Kanda, Direct-bandgap properties and evidence for ultraviolet lasing of hexagonal boron nitride single crystal, *Nat. Mater.* 3 (2004) 404–409.
- [15] M.G. Silly, P. Jaffrennou, J. Barjon, J.-S. Lauret, F. Ducastelle, A. Loiseau, E. Obraztsova, B. Attal-Tretout, E. Rosenthaler, Luminescence properties of hexagonal boron nitride: cathodoluminescence and photoluminescence spectroscopy measurements, *Phys. Rev. B* 75 (2007) 1–5.
- [16] C.W. Chang, A.M. Fennimore, A. Afanasiev, D. Okawa, T. Ikuno, H. Garcia, D. Li, A. Majumdar, A. Zettl, Isotope effect on the thermal conductivity of boron nitride nanotubes, *Phys. Rev. Lett.* 97 (2006) 1–4.
- [17] Y. Xiao, X.H. Yan, J.X. Cao, J.W. Ding, Y.L. Mao, J. Xiang, Specific heat and quantized thermal conductance of single-walled boron nitride nanotubes, *Phys. Rev. B* 69 (2004) 1–5.
- [18] T.A. Hilder, D. Gordon, S.H. Chung, Salt rejection and water transport through boron nitride nanotubes, *Small* 5 (2009) 2183–2190.
- [19] H. Lim, B.L. Suh, M.J. Kim, H. Yun, J. Kim, B.J. Kim, S.G. Jang, High-performance, recyclable ultrafiltration membranes from P4VP-assisted dispersion of flame-resistant boron nitride nanotubes, *J. Membr. Sci.* 551 (2018) 172–179.
- [20] S. Casanova, T.Y. Liu, Y.M.J. Chew, A. Livingston, D. Mattia, High flux thin-film nanocomposites with embedded boron nitride nanotubes for nanofiltration, *J. Membr. Sci.* 597 (2020) 117749.
- [21] X. Chen, P. Wu, M. Rousseas, D. Okawa, Z. Gartner, A. Zettl, C.R. Bertozzi, Boron nitride nanotubes are noncytotoxic and can be functionalized for interaction with proteins and cells, *J. Am. Chem. Soc.* 131 (2009) 890–891.
- [22] R. Arenal, X. Blase, A. Loiseau, Boron-nitride and boron-carbonitride nanotubes: synthesis, characterization and theory, *Adv. Phys.* 59 (2010) 101–179.
- [23] M. Radostavljević, J. Appenzeller, V. Derycke, R. Martel, P. Avouris, A. Loiseau, J.L. Cochon, D. Pigache, Electrical properties and transport in boron nitride nanotubes, *Appl. Phys. Lett.* 82 (2003) 4131–4133.
- [24] D. Lahiri, A. Hadjikhani, C. Zhang, T. Xing, L.H. Li, Y. Chen, A. Agarwal, Boron nitride nanotubes reinforced aluminum composites prepared by spark plasma sintering: Microstructure, mechanical properties and deformation behavior, *Mater. Sci. Eng. A* 574 (2013) 149–156.
- [25] C. Zhi, Y. Bando, C. Tang, S. Honda, H. Kuwahara, D. Golberg, Boron nitride nanotubes/polystyrene composites, *J. Mater. Res.* 21 (2006) 2794–2800.
- [26] M.L. Cohen, A. Zettl, The physics of boron nitride nanotubes, *Phys. Today* 63 (2010) 34–38.
- [27] A. Loiseau, F. Willaime, N. Demonty, G. Hug, H. Pascard, Boron nitride nanotubes with reduced numbers of layers synthesized by arc discharge, *Phys. Rev. Lett.* 76 (1996) 4737–4740.
- [28] Y. Shimizu, Y. Moriyoshi, H. Tanaka, S. Komatsu, Boron nitride nanotubes, webs, and coexisting amorphous phase formed by the plasma jet method, *Appl. Phys. Lett.* 75 (1999) 929–931.
- [29] J. Cumings, A. Zettl, Mass-production of boron nitride double-wall nanotubes and nanococoons, *Chem. Phys. Lett.* 316 (2000) 211–216.
- [30] C.M. Lee, S.I. Choi, S.S. Choi, S.H. Hong, Synthesis of boron nitride nanotubes by arc-jet plasma, *Curr. Appl. Phys.* 6 (2006) 166–170.
- [31] D. Golberg, Y. Bando, M. Eremets, K. Takemura, K. Kurashima, H. Yusa, Nanotubes in boron nitride laser heated at high pressure, *Appl. Phys. Lett.* 69 (2002) 2045–2047.
- [32] D.P. Yu, X.S. Sun, C.S. Lee, I. Bello, S.T. Lee, H.D. Gu, K.M. Leung, G.W. Zhou, Z.F. Dong, Z. Zhang, Synthesis of boron nitride nanotubes by means of excimer laser ablation at high temperature, *Appl. Phys. Lett.* 72 (1998) 1966–1968.
- [33] T. Laude, Y. Matsui, A. Marraud, B. Jouffrey, Long ropes of boron nitride nanotubes grown by a continuous laser heating, *Appl. Phys. Lett.* 76 (2000) 3239–3241.
- [34] R.S. Lee, J. Gavillet, M.L. Chapelle, A. Loiseau, J.-L. Cochon, D. Pigache, J. Thibault, F. Willaime, Catalyst-free synthesis of boron nitride single-wall nanotubes with a preferred zig-zag configuration, *Phys. Rev. B* 64 (2001) 6–9.
- [35] R. Arenal, O. Stephan, J.-L. Cochon, A. Loiseau, Root-growth mechanism for single-walled boron nitride nanotubes in laser vaporization technique, *J. Am. Chem. Soc.* 129 (2007) 16183–16189.
- [36] O.R. Lourie, C.R. Jones, B.M. Bartlett, P.C. Gibbons, R.S. Ruoff, W.E. Buhro, CVD growth of boron nitride nanotubes, *Chem. Mater.* 12 (2000) 1808–1810.
- [37] C.H. Lee, J. Wang, V.K. Kayatsha, J.Y. Huang, Y.K. Yap, Effective growth of boron nitride nanotubes by thermal chemical vapor deposition, *Nanotechnology* 19 (2008).
- [38] M.J. Kim, S. Chatterjee, S.M. Kim, E.A. Stach, M.G. Bradley, M.J. Pender, L.G. Sneddon, B. Maruyama, Double-walled boron nitride nanotubes grown by floating catalyst chemical vapor deposition, *Nano Lett.* 8 (2008) 3298–3302.
- [39] Y. Huang, J. Lin, C. Tang, Y. Bando, C. Zhi, T. Zhai, B. Dierre, T. Sekiguchi, D. Golberg, Bulk synthesis, growth mechanism and properties of highly pure ultrafine boron nitride nanotubes with diameters of sub-10 nm, *Nanotechnology* 22 (2011) 145602.
- [40] Y. Chen, L.T. Chadderton, J.F. Gerald, J.S. Williams, A solid-state process for formation of boron nitride nanotubes, *Appl. Phys. Lett.* 74 (1999) 2960–2962.
- [41] J. Yu, Y. Chen, R. Wuhrer, Z. Liu, S.P. Ringer, In situ formation of BN nanotubes during nitriding reactions, *Chem. Mater.* 17 (2005) 5172–5176.
- [42] J. Yu, B.C.P. Li, J. Zou, Y. Chen, Influence of nitriding gases on the growth of boron nitride nanotubes, *J. Mater. Sci.* 42 (2007) 4025–4030.

- [43] W. Han, Y. Bando, K. Kurashima, T. Sato, Synthesis of boron nitride nanotubes from carbon nanotubes by a substitution reaction, *Appl. Phys. Lett.* 73 (1998) 3085–3087.
- [44] W.Q. Han, W. Mickelson, J. Cumings, A. Zettl, Transformation of $B_xC_yN_z$ nanotubes to pure BN nanotubes, *Appl. Phys. Lett.* 81 (2002) 1110–1112.
- [45] M.W. Smith, K.C. Jordan, C. Park, J. Kim, P.T. Lillehei, R. Crooks, J.S. Harrison, Very long single- and few-walled boron nitride nanotubes via the pressurized vapor/condenser method, *Nanotechnology* 20 (2009) 505604.
- [46] K.S. Kim, C.T. Kingston, A. Hrdina, M.B. Jakubinek, J. Guan, M. Plunkett, B. Simard, Hydrogen-catalyzed, pilot-scale production of small-diameter boron nitride nanotubes and their macroscopic assemblies, *ACS Nano* 8 (2014) 6211–6220.
- [47] K.S. Kim, M. Couillard, H. Shin, M. Plunkett, D. Ruth, C.T. Kingston, B. Simard, Role of hydrogen in high-yield growth of boron nitride nanotubes at atmospheric pressure by induction thermal plasma, *ACS Nano* 12 (2018) 884–893.
- [48] M. Asmann, A. Wank, H. Kim, J. Heberlein, E. Pfender, Characterization of the converging jet region in a triple torch plasma reactor, *Plasma Chem. Plasma Process.* 21 (2001) 37–63.
- [49] K. Ramachandran, H. Nishiyama, Structural analysis of converging jets in a triple torch plasma system, *J. Phys. D Appl. Phys.* 36 (2003) 1198–1203.
- [50] M. Kim, J. Oh, T. Kim, Y.H. Lee, S. Hong, S. Choi, Synthesis of metal boride nanoparticles using triple thermal plasma jet system, *J. Nanosci. Nanotechnol.* 19 (2019) 6264–6270.
- [51] J. Oh, M. Kim, Y.H. Lee, S. Hong, T. Kim, S. Choi, Synthesis of tungsten carbide nanomaterials in triple DC thermal plasma jet system, *J. Nanosci. Nanotechnol.* 19 (2019) 6277–6284.
- [52] T.H. Kim, Y.H. Lee, M. Kim, J.H. Oh, S. Choi, Thermal flow characteristics of the triple plasma torch system for nanoparticle synthesis, *IEEE Trans. Plasma Sci.* 47 (2019) 3366–3373.
- [53] H.B. Levine, Chemical equilibrium in complex mixtures, *J. Chem. Phys.* 36 (1994) 1957–1959.
- [54] J.M. Park, K.S. Kim, T.H. Hwang, H.S. Hong, Three-dimensional modeling of arc root rotation by external magnetic field in nontransferred thermal plasma torches, *IEEE T. Plasma Sci.* 2 (2004) 479–487.
- [55] A.B. Murphy, C.J. Arundell, Transport coefficients of argon, nitrogen, oxygen, argon-nitrogen, and argon-oxygen plasmas, *Plasma Chem. Plasma Process.* 14 (1994) 451–490.
- [56] A.B. Murphy, P. Kovitya, Mathematical model and laser scattering temperature measurement of a direct current plasma torch discharging into air, *J. Appl. Phys.* 73 (1993) 4759–4769.
- [57] S. Choi, D. Park, T. Watanabe, Thermal plasma decomposition of fluorinated greenhouse gases, *Nucl. Eng. Technol.* 44 (2012) 21–32.
- [58] T. Kim, S. Choi, D. Park, Numerical simulation on the influence of water spray in thermal plasma treatment of CF_4 gas, *Curr. Appl. Phys.* 12 (2012) 509–514.
- [59] H.S. Uhm, Generation of various radicals in nitrogen plasma and their behavior in media, *Phys. Plasmas* 22 (2015) 123506.
- [60] S. Agarwal, B. Hoex, M.C.M. Van De Sanden, D. Maroudas, E.S. Aydil, Absolute densities of N and excited N_2 in a N_2 plasma, *Appl. Phys. Lett.* 83 (2003) 4918–4920.
- [61] J. Ma, Y.K. Pu, Tuning the electron temperature of a nitrogen plasma by adding helium and argon, *Phys. Plasmas* 10 (2003) 4118–4122.
- [62] P. André, J. Aubreton, M.F. Elchinger, P. Fauchais, A. Lefort, A new modified pseudoequilibrium calculation to determine the composition of hydrogen and nitrogen plasmas at atmospheric pressure, *Plasma Chem. Plasma Process.* 21 (2001) 83–105.
- [63] A.B. Murphy, Transport coefficients of hydrogen and argon-hydrogen plasmas, *Plasma Chem. Plasma Process.* 20 (2000) 279–297.